Plasma surface modification of single-atom Fe active sites on nano-sized graphene platelets for advanced oxygen reduction reaction

Sungho Lee[1, *], Seonghee Kim[1, *], Jin Hong Lee[2], Heechae Choi[3], Nozomi Takeuchi[4, **], Oi Lun Li[1, **]

[1] School of Materials Science and Engineering, Pusan National University, South Korea
[2] School of Chemical Engineering, Pusan National University, South Korea
[3] Institute of Inorganic Chemistry, University of Cologne, Germany
[4] Department of Electrical and Electronic Engineering, Tokyo Institute of Technology, Japan

* Co-first authors contributed equally to this paper.
** Corresponding author: helenali@pusan.ac.kr (Oi Lun Li), takeuchi@ee.e.titech.ac.jp (Nozomi Takeuchi)

Abstract

Single-atom Fe-doped carbon nanographene demonstrates promising results as an oxygen reduction reaction (ORR) electrocatalyst in fuel cells and rechargeable metal-air batteries. In this study, plasma-in-liquid process was applied to modify the surface of graphene nanoplatelet (GNP) with iron (II) Phthalocyanine as the Fe precursor and mixed into 1-Methyl-2-pyrrolidone (solvent) for 20 minutes. During the plasma modification, tiny discharge bubbles were observed, where the emission of C_2, CH, CN, and H radicals were identified by the optical emission spectrum. From the high-resolution TEM and the corresponding EDS elemental mapping images, the isolated Fe were successfully anchored as single-atom on GNP between 0.50 ~ 0.82 at.%. The ORR activity greatly enhanced after plasma modification, where the single-atom Fe-doped GNP demonstrated extremely high onset potential (E_{onset}) and half-wave potential ($E_{1/2}$) of 0.95−0.98 V and 0.87−0.90 V vs RHE, respectively. Most importantly, plasma-modified Fe-GNP catalysts showed superior ORR catalytic activity compared to other single-atom Fe with similar metal loading catalysts reported in recent studies. The unique plasma-induced chemical reaction *via* active radicals not only successfully anchored atomic Fe onto the surface but also created certain defects of GNP, which created a synergic effect on the ORR catalytic activities.

Keywords: Plasma modification, single-atom doped graphene, oxygen reduction reaction, electrocatalysts.

1. Introduction

The growing demand for green and renewable energy has inspired the vigorous development of fuel cell and metal-air batteries. However, the widespread commercialization of these sustainable energy storage system is hindered by their large overpotentials for the oxygen reduction reaction (ORR) [1]. Commercially, the noble-metal Platinum (Pt) nanoparticles or Pt-rich alloy supported on carbon substrate have been widely used as ORR catalysts [2]. However, the high capital and manufacturing cost of noble Pt catalysts greatly limited their practical applications. In recent years, many efforts have been conducted to find other substitutions of Pt-based catalysts with compatible catalytic activity. Among many attempted materials, single-atom metal-doped carbon materials demonstrate promising results as future ORR catalyst due to their ultra-high atom utilization efficiency and surface-active energy [3]. In the case of the combination of single-atom Fe with nitrogen-doped carbon, it shows the highest effect in comparison to other transition metals [4]. For instance, Zhu *et al*. [5] presented a single-atom Fe ORR electrocatalyst with a high onset and half-wave potential of 0.990 and 0.927 V vs RHE, respectively, in 0.1 M KOH, which was superior to those of commercial Pt/C and other single-

atom metal electrocatalysts. Li *et al.* prepared dense single-atom Fe-N-C electrocatalysts with high density via chemical vapor deposition to fully utilize the Fe-rich ORR active sites for superior ORR activity. This catalyst delivers an unprecedented oxygen reduction reaction activity of 33 mA cm^{-2} at 0.90 V in a H_2–O_2 proton exchange membrane fuel cell at 1.0 bar and 80 °C [6]. A theoretical model was developed to investigate the ORR activity of single-atom Fe-N site from the spatial structure and energy level of the frontier orbitals by density functional theory calculations [7]. The study reported that the Fe–O bond length, the d-band center gap of spin states, the magnetic moment of Fe site and absorbed O_2 as descriptors were important parameters for the advanced ORR activity when utilizing single-atom Fe as active sites.

Despite these achievements, the fabrication of well-dispersed single-atom Fe catalysts remain challenging. Notably, control of the interfacial contact between the metal atoms and the carbon/graphene support are crucial for high ORR activity [8]. The currently known single-atom Fe catalysts are largely synthesized by pyrolysis of transition-metal-based metal-organic frameworks (MOFs) [9-10]. Rigid structures like zeolite imidazole frameworks or functionalized carbons with oxygenated groups should be used as supports to immobilize metal ions, and thus prevent the aggregation of metal species during thermal treatment [11-12]. Although these methods allow one to obtain carbon matrices with various atomically dispersed metal centers, they require numerous steps and tedious processes to synthesize appropriate precursors, and the corresponding carbonization ratios and production rates remain low [13]. Consequently, a noble strategy of incorporating single-metal atoms under room temperature is essential to prevent the aggregation of these atoms into clusters.

Recently, plasma-in-liquid process has been accepted as a novel modification route for carbon-based materials mainly due to the recent development of various plasma sources operated from low to atmospheric pressures. During plasma discharge, various types of electrons and radicals are generated and the unique plasma–liquid interfaces initiate multiple physical and chemical processes [14]. Shirafuji *et al.* has reported surface functionalization of multi-walled carbon nanotube (MWCNTS) in ammonia aqueous solution without any chemical or surfactant addition [15]. Li *et al.* have applied a similar process to modify carbon black (CB) with -OH, -COOH, -SO$_3$H sites with high acidic and -SO$_3$H densities under dilute sulfuric acid [16]. The mechanism of carbon sulfonation was expected to be initiated by H radicals in sulfuric acid and generated active SO$_3$ (g). Then, active SO$_3$ groups aggressively attacked the surface of carbon and formed -HSO$_3$ on the surface. In addition, the formation of -COOH and phenolic –OH also simultaneously occurred due to the presence of O and OH radicals. Takeuchi *et al.* also applied the plasma process in water-ethanol mixed solution for the chemical reduction of graphene oxide powders [17]. The fraction of ethanol was varied from 0 to 75 vol.%, and the most effective reduction was obtained with 25 vol.% ethanol. They concluded that ethanol radical is the key species in the reduction process as well as the reduction of gold chloride ions [18].

In this study, we applied liquid-in-plasma to modify the surface of graphene nanoplatelet (GNP) with atomic Fe active sites for the first time. GNP was selected as the carbon supporting materials in ORR application due to its' high conductivity and relatively large surface area. A non-equilibrium plasma-in-liquid process was controlled with a discharge voltage, current, and frequency in the range of 1 kV, 1 × 10 A, and 10^3–10^4 kHz, respectively. The detail of plasma discharge and its phenomena were first characterized, followed by the materials analyses and the electrochemical performance of the plasma-modified single-atom Fe-doped electrocatalysts. This study aims to expand the application of plasma surface modification on energy materials in near future.

2. Experimental

2.1 Plasma experimental setup and parameter

The schematic of the plasma reactor and its electrical circuit is shown in Fig. 1. A bipolar pulsed power supply (Kurita Co. Ltd., MPP04-A4-200, Kyoto, Japan) was used as the power source. The set values of the bipolar power supply for voltage, pulse frequency, and pulse width were 4 kV, 25 kHz, 0.15 μs, respectively. The electrode distance was maintained at 1 mm. The applied voltage to the high voltage (H.V.) electrode, V, and the current flowing through the reactor, I, were measured using a H.V. probe (Tektronix, P6015A) and a current transformer (CT) (Pearson Electronics, Model 4100), respectively. The waveforms were monitored and sampled by an oscilloscope (Tektronix, MDO3104). The energy consumed during one period in the reactor, E_{pulse} [J], is calculated using equation (1) as:

$$E_{\text{pulse}} = \int_0^T VI dt \qquad (1)$$

where, $T\,(=1/f)$ is the period of the applied voltage and f is the pulse repetition frequency. The time averaged power, P_{ave} [W], is obtained by equation (2) as:

$$P_{\text{ave}} = f E_{\text{pulse}} \qquad (2)$$

The characteristics of the plasma in liquid were investigated by monitoring the voltage and current waveforms and observed using an intensified CCD (ICCD) camera (Princeton Instruments, PI-MAX). Optical emission spectroscopy (OES) was conducted with a spectrometer (Ocean Optics, FLAME-S-UV-VIS-ES) by inserting the optical fiber into the solution. Light emission from the plasma could not pass through the solution with a high concentration of FePc. Thus, the observation using ICCD and OES was conducted at a FePc concentration of 0.2 g L^{-1} to make the emission visible.
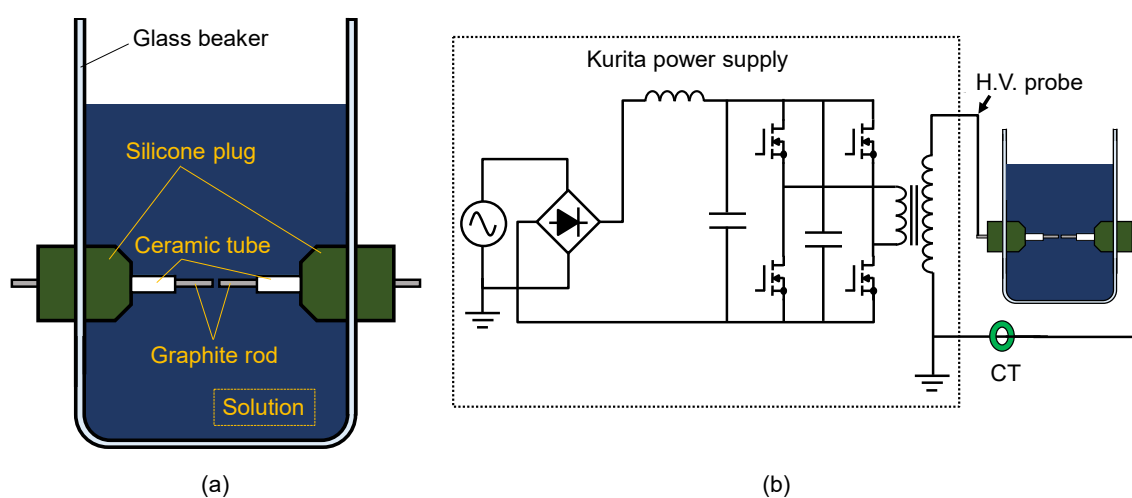
Fig. 1. Schematics of (a) plasma reactor and (b) its electric circuit.

2.2 Plasma surface modification of Fe-doped graphene platelet (Fe-GNP)

A precursor solution was prepared for by mixing 100 mg and 200 mg of Iron (II) Phthalocyanine (FePc, Dye content 97%, Sigma-Aldrich) into 100 mL of 1-Methyl-2-pyrrolidone (NMP, 99.0% purity, Fujifilm Wako Chemical). Graphene nanoplatelet (GNP, Sigma-Aldrich, < 2 µm particle size, 750 $m^2\,g^{-1}$ specific surface area, 2×10^6 S m^{-1} electrical conductivity) was considered to be the variable parameters in this experiment and was added into the catalysts precursor, which resulted in the varying the mass ratio between the catalytic active site (FePc) and the substrate (GNP) as 2:1 and 1:1, respectively. The catalysts prepared with GNP of 100 mg and 200 mg were denoted as Fe-GNP(2:1) and Fe-GNP(1:1) hereafter. In addition, pristine GNP without plasma modification (named as GNP) was used as reference materials for the characterization and electrochemical performance.

Plasma surface modification was operated with a pair of Φ2.0 mm 99.99% graphite electrodes (GoodFellow, Seoul, Korea), which were insulated by ceramic tube, then processed for 20 mins. Finally, the plasma-modified GNP was filtered through the Φ55-mm polytetrafluoroethylene filter and washed with ethanol and D. I. water until the filtered solution became transparent. Finally, filtered GNP was dried at 80-degree oven overnight to remove residual solution.

2.3 Materials and electrochemical characterization

The morphology and structure of plasma-treated GNP were analyzed by X-ray diffraction (XRD, Rigaku, Ultima IV, Tokyo, Japan) and transmission electron microscopy (TEM, Thermo Fisher Scientific, TALOS F200X, Seoul, Korea). An electrochemical potentiostat (Biologic, VSP, Grenoble, France) was used to analyze

the catalytic activity of the plasma-treated GNP and 20 wt.% Pt/C (Fuelcell store, 20% Platinum on Carbon XC-72) in 0.1 M KOH. The catalyst ink for the electrochemical analysis was composed of 8 mg of well-ground plasma-treated GNP in a mixed solution of distilled water (480 μL), ethanol (480 μL), and Nafion®117 solution (40 μL) ultrasonicated for 30 min. The well-dispersed catalyst ink (600 μg cm^{-2}) was dropped on a well-polished glassy carbon disk electrode (4 mm diameter) to prepare the working electrode. Simultaneously, a platinum coil counter electrode was used together with a Hg/HgO (1 M NaOH) reference electrode for the 0.1 M KOH electrolyte to establish a standard three-electrode cell system for electrochemical performance. The catalytic activity of ORR was measured by linear sweep voltammetry (LSV) in O$_2$-saturated 0.1 M KOH and alkaline seawater electrolytes at a scan rate of 5 mV s^{-1}, rotating speed of 1600 rpm, and a potential range from 0.2 to 1.0 V vs. RHE in 0.1 M KOH. Cyclic voltammetry (CV) was performed at 50 mV s^{-1} over a potential range from 0.1 to 1.2 V vs. RHE in 0.1 M KOH.

3. Results and discussion

3.1 Observation of plasma modification process

Fig. 2 depicts the typical waveforms of voltage and current; (a) for both positive and negative polarities and (b) extended for positive polarity. Discharges were initiated during the rising edges of the applied voltage in both polarities at approximately ± 1.0–1.7 kV. Then, the voltage dropped to the discharge sustaining voltage of approximately 200 V, and a discharge current with a peak of 7 A flowed. E_{pulse} obtained as an averaged value of three-times measurements was 0.36 mJ with the standard variation of 0.11 mJ, which corresponded to P_{ave} of 9.0 W.
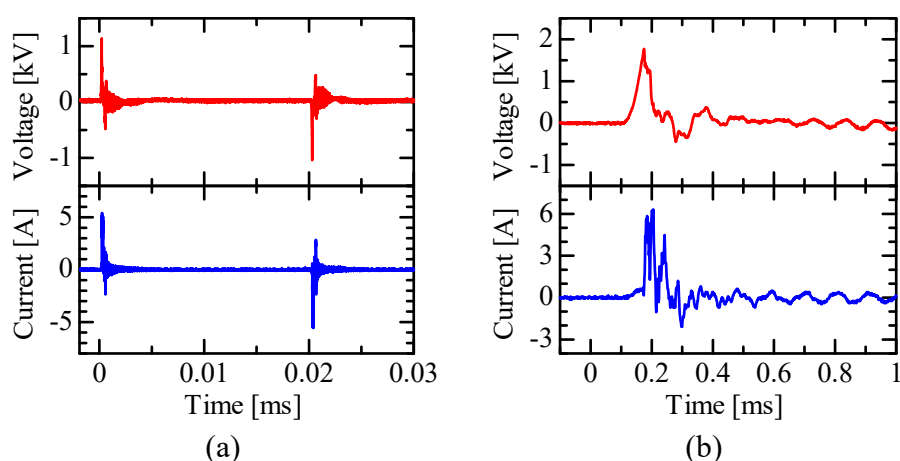
Fig. 2. Typical waveforms of voltage and current, (a) with both positive and negative polarities, (b) extended for positive polarity.

An image of the plasma obtained with the ICCD camera is shown in Fig. 3 (a). The exposure time was set at 0.04 ms, thus the emission during one period was observed. Because of the generation of small bubbles by solution evaporation, it was difficult to see the emission clearly, but we can confirm that a filamentary discharge plasma with a diameter of approximately 150 μm was generated. The position of the filamentary discharge plasma was not fixed. The plasma moved along the electrode surfaces with generation of bubbles. Fig. 3 (b) depicts the OES spectrum and detects the emission from C$_2$, CH, CN and H radicals originated from the organic solvent. Although there should be strong emission between 600–700 nm, the light emission in this range was absorbed mostly by the solution. When tungsten rods were used instead of the graphite rods as the electrodes, similar spectra were observed, therefore, these radicals were originated in the solution. Such emissions of CH and C$_2$ were previously observed in plasma-in-liquid processes using different organic solvents [19-20]. On the other hand, Fe peaks were not detected due to the extremely low concentration of its precursor (0.2 g L^{-1}) compared to the solvent (1-Methyl-2-pyrrolidone). In addition, the planar Fe-N$_4$ structure in FePc has relatively high chemical and thermal stability [21], and the strong Fe-N$_4$ bonding was fully

maintained during similar plasma condition [22]. Therefore, we expected that molecular structure of Fe-N$_4$ was anchored on GNP without breaking the Fe-N bonding.
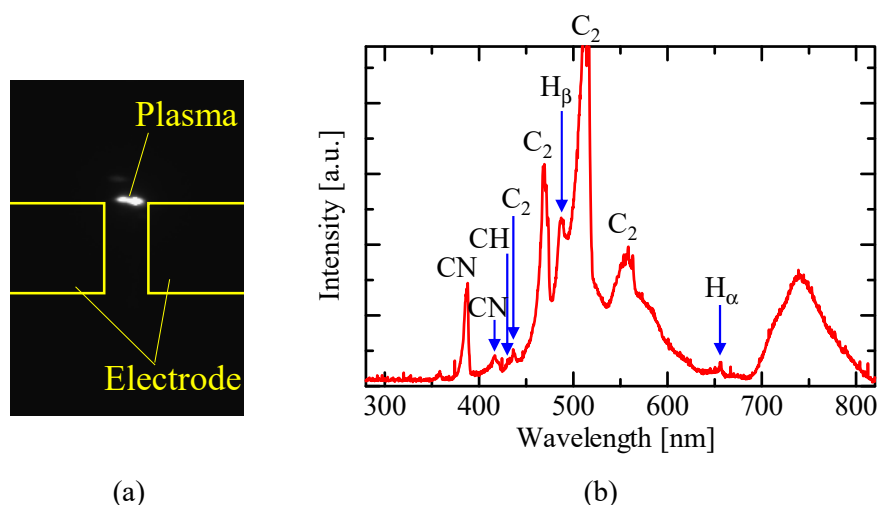
Fig. 3. (a) Image of plasma captured by an ICCD camera, (b) optical emission spectrum.

3.2 Material characterizations of Plasma-modified Fe-GNP

The XRD patterns of pristine GNP, plasma-modified Fe-GNP(1:1), and Fe-GNP(2:1) were first compared to identify the presence of crystalline metal particles after plasma modification. As shown in Fig. 4 (a), all XRD patterns feature similar broad peaks at 23° and 43°, which were indexed to the (002) and (101) planes of graphitic carbon, respectively. Notably, no peaks attributable to crystalline metal nanoparticles were detected. The defect of the graphene plane in GNP after plasma modification can be revealed by Raman spectroscopy. In Fig. 4 (b), the Raman spectra of pristine GNP, plasma-modified Fe-GNP(1:1), and Fe-GNP(2:1) featured two major characteristic peaks, the D-band (1344 cm^{-1}) and the G-band (1587 cm^{-1}). However, the distinct peaks become broader with the introduction of FePc, which indicates that the introduction of single-atom Fe creates more defects in the GNP. Moreover, the D-band and G-bank peaks turn to two board peaks in Fe-GNP (2:1). It is reasonable that the doping amount of single atom Fe increases with a higher concentration of FePc introduced into the precursor.
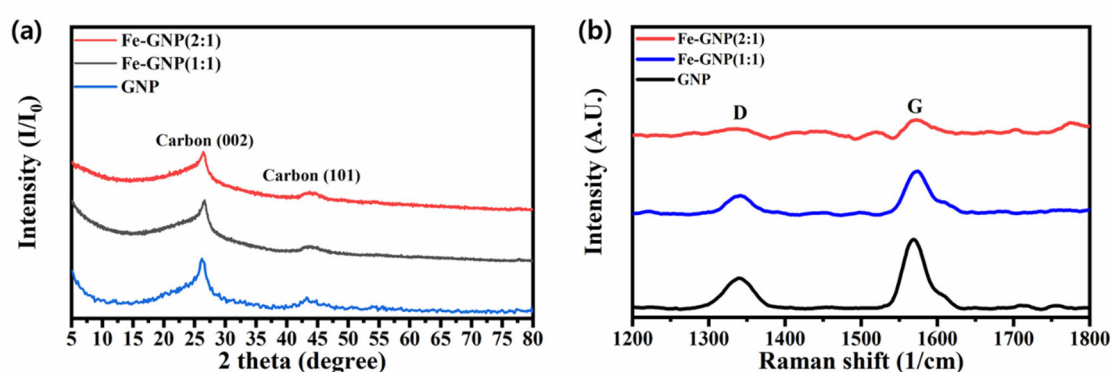
Fig. 4. (a) XRD patterns and (b) Raman spectra of pristine GNP, Fe-GNP(1:1) and Fe-GNP(2:1).

High-resolution transmission electron microscopy TEM images (bright field) demonstrate the microstructures of the plasma-modified Fe-GNP(2:1) in Fig. 4 (a) – (c). The nano-graphene platelets are stacked with over 10 layers of graphitic carbon layers with a lattice spacing of ~0.34 nm directed toward the (002) plane and show an average length of 20 nm. Even under HR-TEM image in Fig. 4 (c), no metal nanoparticles can be found. This observation agrees with that of the XRD pattern, where plasma modification did not synthesize metal nanoparticles from FePc precursors. On the other hand, aberration-corrected high-

angle annular dark-field scanning transmission electron microscopy (HAADF-STEM) images (Fig. 4 (d)) and its corresponding EDS elemental mapping images (Fig. 4 (e) – (g)) reveal the presence of isolated C, Fe and N atoms. The relative atomic percentage (at.%) of Fe-GNP(1:1) and Fe-GNP(2:1) are summarized in Table 1. Based on the EDS mapping results, it can be confirmed that Fe and N are successfully anchored on GNP between 0.50 ~ 0.82 at.% and 2.38 ~ 2.46 at.%, respectively, after plasma surface modification. The presence of oxygen in both catalysts is generally formed by the surface carbon oxidation under air atmosphere.
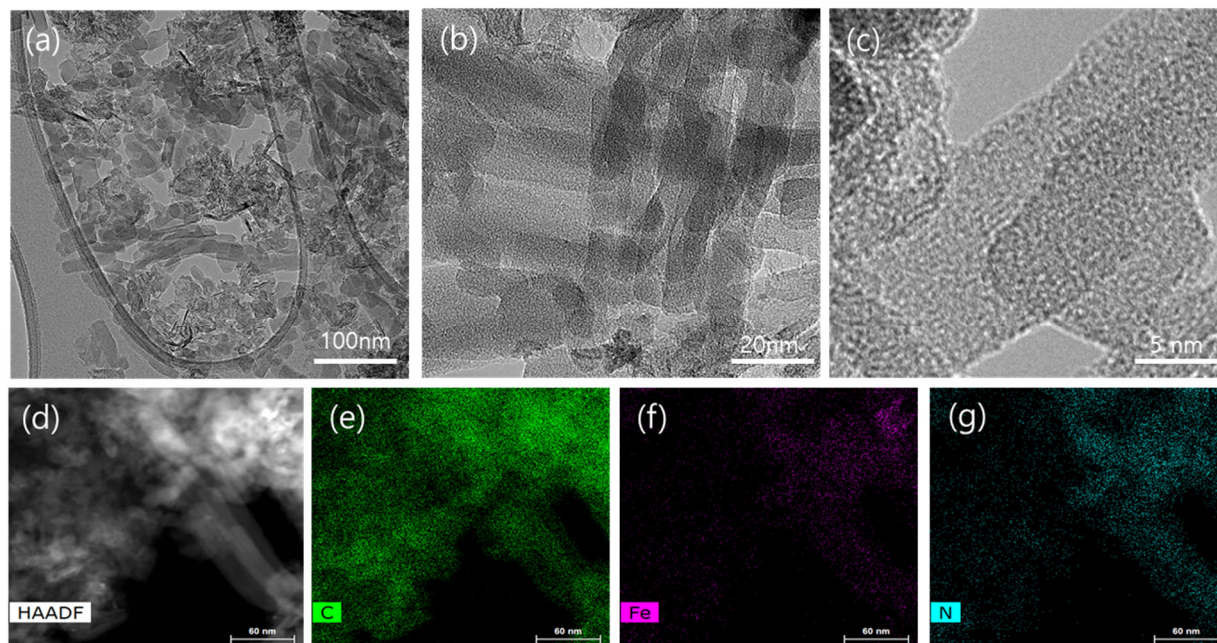
Fig. 5. (a-c) Bright-field TEM images, (d) Aberration-corrected HAADF-TEM image of Fe-GNP(2:1) Elemental mapping of (e) C, (f) Fe and (g) N corresponding to (d).

Table 1. Elemental Mapping results of plasma-modified Fe-GNP.

	C (at.%)	Fe (at.%)	N (at.%)	O (at.%)
Fe-GNP (1:1)	90.81	0.50	2.38	6.34
Fe-GNP (2:1)	87.71	0.72	2.40	9.17

3.3 Catalytic activity of oxygen reduction reaction of Plasma-modified Fe-GNP

The CV of three catalysts in Fig. 6 (a) – (c) under nitrogen and oxygen-saturated conditions with 0.1 M KOH electrolyte were firstly compared to confirm the presence of ORR. The CV of pristine GNP in Fig. 6 (a) shows the very limited activity of ORR since only a small cathodic peak between the 0.6 V and 0.8 V vs RHE is present under saturated oxygen environment. Comparatively, Fe-GNP(1:1) and Fe-GNP(2:1) exhibit two distinct peaks between 0.6 to 1.0 V vs RHE under saturated oxygen condition. The former is indexed to the reduction/oxidation peaks of Fe^{3+}/Fe^{2+}, the latter is signed to redox couple of Fe^{2+}/Fe^+ [23]. With the increase of the doping of single atom FeN_4 in Fe-GNP (2:1), the reduction peak shift towards more positive potential (~1.0 V vs RHE), suggesting the increased number of active sites enhance the ORR activity of GNP. The linear sweep voltammograms in Fig. 6 (d) show that the ORR onset potential (E_{onset}) and half-wave potential ($E_{1/2}$) of the pristine GNP merely exhibit a low value of 0.8 and 0.75 V vs RHE, respectively. On the contrary, the ORR activity greatly enhanced after plasma modification, where Fe-GNP(1:1) and Fe-GNP(2:1) demonstrate extremely high E_{onset} and $E_{1/2}$ of 0.95 and 0.87 V vs. RHE, and 0.98 and 0.90 V vs RHE, correspondingly. Based on the elemental mapping results, the active sites in Fe-GNP(2:1) are slightly higher than that of Fe-GNP(1:1). Therefore, it is reasonable that the prior catalyst exhibit slightly better ORR performance. These findings prove the importance of single-atom Fe as efficient ORR active sites despite their low content (< 1.0 at.%).

The LSV curves recorded at rotation rates of 400 – 2000 rpm in Fig. 6 (e) were used to further examine the ORR activity and the electron transfer number (*n*) of Fe-GNP(2:1). Linearity and parallel of the plots are

usually considered as an evidence of first-order reaction kinetics with respect to the concentration of dissolved oxygen. The kinetic parameters can be analysed by the Koutecky-Levich equations [24].

$$1/j = 1/j_L + 1/j_k \qquad\qquad (3)$$

$$1/j = 1/B\omega^{1/2} + 1/j_k \qquad\qquad (4)$$

$$B = 0.62\, n\, F\, C_0^*\, D_0^{2/3}\, v^{-1/6} \qquad\qquad (5)$$

where j is the measured current density, j_k and j_L are the kinetic and diffusion-limiting current densities, ω is the rotation rate of disk in the radian ($\omega = 2\pi N$, N is the linear rotation speed), F is the Faradays constant ($F = 96485$ C), n is the number of electrons transferred per oxygen molecule, C_0^* and D_0 are the oxygen bulk concentration (1.2×10^{-6} mol cm^{-3}) and diffusion coefficient of O_2 (1.9×10^{-5} cm^2 s^{-1}), respectively, and v is the kinematic viscosity of electrolyte (1.1×10^{-2} cm^2 s^{-1}).

The direct 4-electron ORR reaction steps (I–IV) corresponding to OOH, O, and OH adsorption and H_2O generation are described as follows [25]:

$$(\text{I})\ O_2(g) + H^+ + e^- \rightarrow OOH^* \qquad\qquad (6)$$

$$(\text{II})\ OOH^* + H^+ + e^- \rightarrow O^* \qquad\qquad (7)$$

$$(\text{III})\ O^* + H^+ + e^- \rightarrow OH^* \qquad\qquad (8)$$

$$(\text{IV})\ OH^* + H^+ + e^- \rightarrow H_2O(l) + {}^* \qquad\qquad (9)$$

where * represents the adsorbed species on the catalyst's surface.

Fig. 6 (f) shows the obtained currents with respect to different rotating speed plotted in the corresponding Koutecky-Levich plots (j^{-1} vs $\omega^{-1/2}$). The electron transfer numbers were calculated from the slope of the Koutecky-Levich plot at each potential. As shown in the mentioned figure, the electron transfer numbers (n) calculated from Koutecky-Levich plots are approximately 4.0 between the potential range of 0.4 to 0.6 V vs RHE. According to the results, Fe-GNP(2:1) demonstrates a direct 4-electron transfer process and again confirms that the incorporation of Fe-N$_4$ active site significantly enhances the ORR activity of GNP. The doping concentration and electrochemical performance of other reported single-atom Fe doped carbon catalysts are summarized in Table 2. Since single-atom Fe are the major active sites for the ORR reaction, the catalytic activities with low Fe loading (0.7 at.%) were hardly over 0.82 V vs RHE [26−27]. On the other hand, the ORR activity drastically enhanced to above 0.89 V vs RHE with higher loading of single-atom Fe of around 4 at.% active sites [28]. Comparatively, plasma-modified Fe-GNP catalysts show much superior ORR catalytic activity with E$_{1/2}$ over 0.90 V vs RHE compared to other low single-atom Fe loading catalysts. The unique plasma-induced chemical reaction *via* active radicals not only successfully anchor atomic Fe onto the surface but also created certain defects of GNP, which might be beneficial in the enhancement of electronic transfer and ORR catalytic activities.

Table 2. Comparison of recently reported Fe single-atom doped carbon electrocatalysts.

Electrocatalysts	ORR half-wave potential (E$_{1/2}$)	Single-atom Fe loading	Reference
FeNC-S-MSUFC	0.73 V vs RHE	0.5 at.%	[26]
Fe-NCCs and PANI-Fe-C	0.80–0.82 V vs RHE	0.20–0.26 at.%	[27]
FeN$_x$-PNC	0.89 V vs RHE	3.94 at.%	[28]
Fe-GNP(1:1)	**0.87 V vs RHE**	**0.50 at.%**	**This work**
Fe-GNP(2:1)	**0.90 V vs RHE**	**0.72 at.%**	**This work**
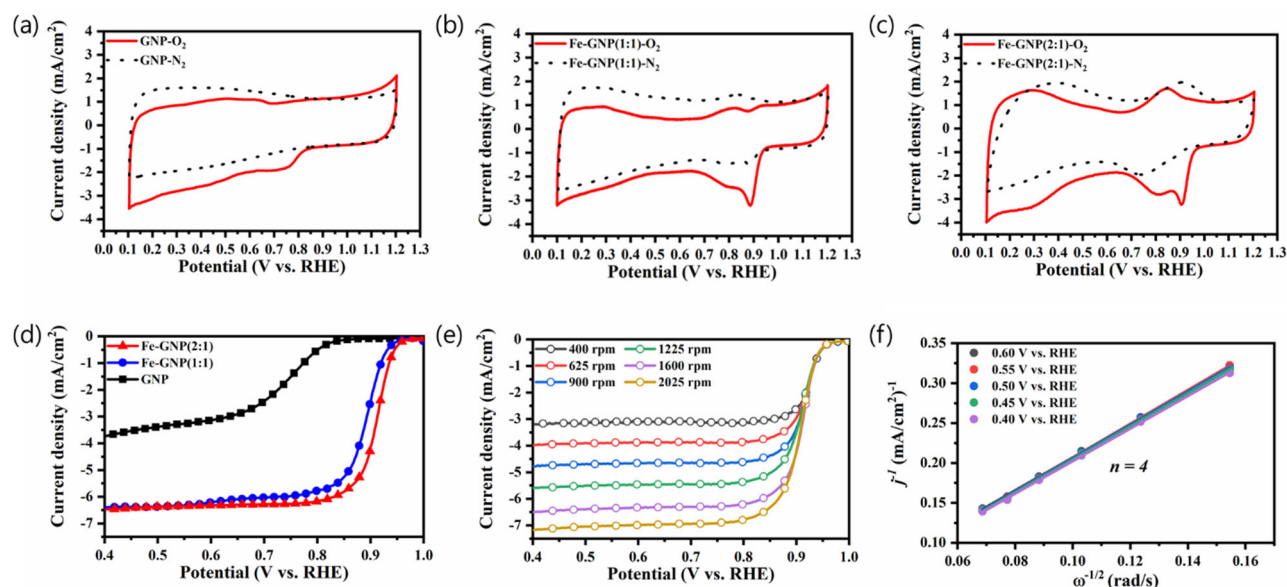
Fig. 6. CV curves recorded in O_2-saturated (red line) and N_2-saturated (black line) in 0.1 M KOH solution at a scan rate of 50 mV/s of (a) pristine GNP, (b) plasma-modified Fe-GNP(1:1) and (c) plasma-modified Fe-GNP(2:1). (d) LSV curves of pristine GNP, plasma-modified Fe-GNP(1:1) and Fe-GNP(2:1) in O_2-saturated 0.1 M KOH solution at 1600 rpm with 5 mV s^{-1}. (e) LSV curves of Fe-GNP (2:1) with different rotating speeds between 400 – 2025 rpm. (f) Koutecky-Levich plots and transferred electron number derived from RDE measurement at various potentials between 0.40 to 0.60 V vs RHE.

6. Conclusion

In this research, we have applied plasma-in-liquid to modify the surface of graphene nanoplatelet with single-atom Fe active sites. Non-equilibrium plasma-in-liquid discharges were initiated and the sustaining voltage and the peak discharge current were approximately 200 V and 7 A, respectively. The average energy per pulse (E_{pulse}) was 0.36 mJ, which corresponded to a power average (P_{ave}) of 9.0 W. From the ICCD camera, generation of filamentary discharge plasma accompanied with generation of bubbles was confirmed where the emission from C_2, CH, CN and H radicals originated from the organic solvent were identify *via* the OES spectrum. On the other hand, emission corresponding to excited Fe was not detected due to the extremely low concentration of FePc precursor. From materials characterization, the images from high-resolution transmission electron microscopy revealed the presence of isolated C, Fe, and N atoms, and the relative atomic percentage Fe and N were $0.50 \sim 0.82$ at.% and $2.38 \sim 2.46$ at.%, respectively. The results from electrochemical performance also showed that the reduction peak shifted towards more positive potential (~1.0 V vs RHE) with increasing amount of single-atom Fe active site in Fe-GNP (2:1). The ORR onset potential (E_{onset}) and half-wave potential ($E_{1/2}$) greatly enhanced after plasma modification, where Fe-GNP(1:1) and Fe-GNP(2:1) demonstrated high E_{onset} and $E_{1/2}$ of 0.95 and 0.87 V vs. RHE, and 0.98 and 0.90 V vs RHE, correspondingly, which were much superior to that of pristine GNP. The electron transfer numbers (n) calculated from Koutecky-Levich plots were approximately 4.0 between the potential range of 0.4 to 0.6 V vs RHE. Therefore, the incorporation of the Fe-N_4 active site significantly enhances the ORR activity of GNP and promotes a direct 4-electron transfer ORR process. Compare to other single-atom Fe doped carbon ORR catalysts, plasma modified Fe-GNP catalysts show better ORR catalytic activity with $E_{1/2}$ over 0.90 V vs RHE with similar single-atom Fe loading. The unique plasma-induced chemical reactions *via* active radicals not only successfully anchor atomic Fe onto the surface but also created certain defects of GNP, which might be beneficial in the enhancement of electronic transfer and ORR catalytic activities. Therefore, this study is expected to provide a significant impact on applying plasma surface modification to the field of energy materials in near future.

Acknowledgment

References

[1] Wang, X., Li, Z., Qu, Y., Yuan, T., Wang W., Wu, Y., Li Y., Review of metal catalysts for oxygen reduction reaction: From nanoscale engineering to atomic design, *Chem*, Vol. 5 (6), pp. 1486–1511, 2019.

[2] Shao, M., Chang, Q., Dodelet, J.P. and Chenitz, R., Recent advances in electrocatalysts for oxygen reduction reaction. *Chem. Rev.*, Vol. 116, pp. 3594−3657, 2016.

[3] Li, H., Zhu, H., Zhuang, Z., Lu, S., Fuan, F. and Du, M. Single-atom catalysts for electrochemical clean energy conversion: recent progress and perspectives, *Sus. Energy Fuels*, Vol. 4, pp. 996−1011, 2020.

[4] Song, X., Chen, S., Guo, L., Sun, Y., Li, X., cao, X., Wang, Z., Sun, J., Lin, C. and Wang Y., General dimension-controlled synthesis of hollow carbon embedded with metal singe atoms or core–shell nanoparticles for energy storage applications, *Adv. Energ. Mater.*, Vol. 8 (27), 1801101, 2018.

[5] Zhu, C., Shi, Q., Xu, B. Z., Fu, S., Wan, G., Yang, C., Yao, S., Song, J., Zhou, H., Du, D., Beckman, S.P. Su, D. and Lin, Y., Hierarchically porous M-N-C (M = Co and Fe) single-atom electrocatalysts with robust M-Nx Active Moieties enable enhanced ORR performance, *Adv. Energy Mater.*, Vol. 8 (29), 1801956, 2018.

[6] Jiao, L., Li, J., Richard, L.L, Sun, Q., Strcensky, T., Liu, E., Sougrati, M.T., Zhao, Z., Yang, F., Zong, S., Xu. H., Mukerjee. S., Huang, Y., Cullen, D.A., Park., J. H., Ferrandon, M., Myers, D.J., Jaouen, F. and Jia Q., Chemical vapour deposition of Fe–N–C oxygen reduction catalysts with full utilization of dense Fe–N$_4$ sites, *Nature Mater.*, Vol. 20, pp. 1385−1391, 2021.

[7] Liu. K, Fu. J, Lin, Y., Luo. T., Ni, G., Li, H., Lin, Z. and Liu, M. Insights into the activity of single-atom fe-N-C catalysts for oxygen reduction reaction, *Nature Comm.,* Vol. 13, pp. 2075−2083, 2022.

[8] Ji, S., Chen, Y., Wang, X., Zhang, Z., Wang, D. and Li Y., Chemical synthesis of single atomic site catalysts, *Chem. Rev.,* Vol. 120 (21), pp. 11900−11955, 2020.

[9] Han, X. P., Ling, X. F., Yu, D. S., Xie, D. Y., Li, L. L., Peng, S. J., Zhong, C., Zhao, N. Q., Deng, Y. D. and Hu W. B., Atomically dispersed binary Co–Ni sites in nitrogen–doped hollow carbon nanocubes for reversible oxygen reduction and evolution, *Adv. Mater.,* Vol. 31, 1905622, 2019.

[10] Han, X. P., Ling, X. F., Wang, Y., Ma, T. Y., Zhong, C., Hu, W. B. and Y. D. Deng., Spatial isolation of zeolitic imidazole frameworks–derived cobalt catalysts: from nanoparticle, atomic cluster to single atom., *Angew. Chem. Int. Ed.,* Vol. 58, pp. 5359–5364, 2019.

[11] Wang, T. T., Kou, Z. K., Mu, S. C., Liu, J. P., He, D. P., Amiinu, I. S., Meng, W., Zhou, K., Luo, Z. X., Chaemchuen, S. and Verpoort F., 2D dual–metal zeolitic–imidazolate–framework–(ZIF)–derived bifunctional air electrodes with ultrahigh electrochemical properties for rechargeable zinc–air batteries, *Adv. Funct. Mater.*, Vol. 28 (5), 1705048, 2018.

[12] Lam E. and Luong J. H. T., Carbon materials as catalyst supports and catalysts in the transformation of biomass to fuels and chemicals, *ACS Catal.* Vol. 4 (10), pp.3393–3410, 2014.

[13] Liu, M. M., Wang, L. L., Zhao, K. N., Shi, S. S., Shao, Q. S., Zhang, L., Sun, X. L., Zhao, Y. F. and Zhang J. J., Atomically dispersed metal catalysts for the oxygen reduction reaction: synthesis, characterization, reaction mechanisms and electrochemical energy applications, *Energy Environ. Sci.*, Vol. 12, pp. 2890–2923, 2019.

[14] Takai, O., Solution plasma process (SPP), *Pure Appl. Chem.*, Vol. 80 (9), pp. 2003–2011, 2008.

[15] Shirafuji, T., Nguchi Y., Yamamoto, T., Hieda, J., Saito, N., Takai, S., Tsuchimoto, A., Nojima, K. and Okabe, Y., Functionalization of multiwalled carbon nanotubes by solution plasma processing in ammonia aqueous solution and preparation of composite material with polyamide 6, *Jap. J. App. Phys.,* Vol. 52 (12), 125101, 2013.

[16] Li. O.L., Ikura R. and Ishizaki T., Hydrolysis of cellulose to glucose over carbon catalysts sulfonated via a plasma process in dilute acids, *Green Chem.,* Vol. 19, pp. 4774−4777, 2017.

[17] Takeuchi. N., Kawahara. K.., Gamou. F., Li O.L., Observation of solution plasma in water-ethanol mixed solution for reduction of graphene oxide., *Int. J. Plasma Environ. Sci. Technol.*, Vol. 14, e01009, 2020.

[18] Sudare T., Ueno T., Watthanaphanit A., and Saito N., Accelerated nanoparticles synthesis in alcohol–water-mixture-based solution plasma, *Phys. Chem. Chem. Phys.,* Vol. 17 (45), pp. 30255−30259, 2015.

[19] Morishita, T., Ueno, T., Panomsuwan, G., Hieda, J., Yoshida, A., Bratescu, M.A. and Saito N., Fastest formation routes of nanocarbons in solution plasma processes, *Sci. Rep.* Vol. 6, 36880, 2016.

[20] Li. O. L, Chiba, S., Wada, Y., Panomsuwan, G. and Ishizaki, T., Synthesis of graphitic-N and amino-N in nitrogen-doped carbon via a solution plasma process and exploration of their synergic effect for advanced oxygen reduction reaction, *J. Mater. Chem. A.*, Vol. 5, pp. 2073–2083, 2017.

[21] Ghani, F., Kristen, J. and Rieler, H., Solubility properties of unsubstituted metal phthalocyanines in different types of solvents, *J. Chem. Eng. Data,* Vol. 57 (2), pp. 439–449, 2012.

[22] Chen, K., Kim, S., Je, M., Choi. H., Shi, Z., Vladimir., Kim K.H. and Li O.L., Ultrasonic plasma engineering toward facile synthesis of single-atom M-N$_4$/N-doped carbon (M = Fe, Co) as superior oxygen electrocatalyst in rechargeable zinc-air batteries, *Nano-Micro Lett.*, Vol. 13, pp. 60–80, 2021.

[23] Zhang N. and Liu M., Iron phthalocyanine with coordination induced electronic localization to boost oxygen reduction reaction*, Nature Comm*., Vol. 11, pp. 4173− 4181, 2020.

[24] Wang J., Zhao, C-X., Liu J-N., Ren, D., Li, B-Q., Huang J-Q. and Zhang, Q., Quantitative kinetic analysis on oxygen reduction reaction: A perspective, *Nano Mater. Sci.,* Vol. 3 (3), pp. 313–318, 2021.

[25] Kim, S., Ji, S., Yang, H., Son, H., Choi, H., Kang, J., Li, O.L., Near surface electric field enhancement: Pyridinic-N rich few-layer graphene encapsulating cobalt catalysts as highly active and stable bifunctional ORR/OER catalyst for seawater batteries, *App. Catal. B: Environ*., Vol. 310, 121361, 2022.

[26] Mun, Y., Lee, S., Kim, K., Kim, S., Lee, S., Han, J. W. and Lee J., Versatile strategy for tuning ORR activity of a single Fe-N$_4$ site by controlling electron–with drawing/donating properties of a carbon plane, *J. Am. Chem. Soc.,* Vol. 141 (15), pp. 6254−6260, 2019.

[27] Chung, H. T., Cullen, D. A., Higgins, D., Sneed, B. T., Holby, E. F., More, K. L. and P. Zelenay. Direct atomic–level insight into the active sites of a high–performance PGM-free ORR catalyst. *Science* Vol. 357 (6350), pp. 479–484, 2017.

[28] Ma, L. T., Chen, S. M., Pei, Z. X., Huang, Y., Liang, G. J., Mo, F. N., Yang, Q., Su, J., Gao, Y. H., Zapien, J. A. and Zhi. C. Y., Single–site active iron–based bifunctional oxygen catalyst for a compressible and rechargeable zinc–air battery, *ACS Nano,* Vol. 12 (2), pp. 1949–1958, 2018.